Sriwijaya Journal of Environment
Article
ojs.pps.unsri.ac.id

Assessing the Characteristic of Bands Combination in Log Ratio Change Detection Using SAR Imagery

Agus Dwi Hartanto[1*], Dwi Setyawan[2], Ferdinand Hukama Taqwa[3]

[1]*Postgraduate Student of Environmental Management, Sriwijaya University, Indonesia*
[2] *Soil Science Department, Faculty of Agriculture, Sriwijaya University, Ogan Ilir, Indonesia*
[3]*Aquaculture Department, Faculty of Agriculture, Sriwijaya University, Ogan Ilir, Indonesia*
**Corresponding Author: dwiunsri@yahoo.co.id*

Article history

Received	Received in revised form	Accepted	Available online
09 November 2025	09 December 2025	16 December 2025	21 December 2025

Abstract: Log ratio is one of the change detection techniques often used in SAR image-based flood inundation analysis, where the differences in characteristics between its polarizations are expected to complement each other and provide optimal predictions. This research aimed to identify the characteristics of the output generated from various potential combinations utilizing log ratio change detection and to evaluate the most reliable combination for detecting flood inundation. The study utilized Sentinel-1 GRD IW dual polarization mode before and during the flood event as its main data source. Briefly, the data processing consists of preprocessing, collocation, and change detection, which were subsequently followed by analysis and evaluation. The analysis results indicated a highly significant difference in characteristics among the four outputs of log ratio change, where the combinations of LR_1 and LR_2 detected much smaller changes compared to the combinations of LR_4 and LR_3. The LR_4 combination acts as a counterpoint to the LR_3 combination, as the changes identified in LR_3 showed a tendency towards positive values, whereas the opposite is true for LR_4. The evaluation results show that CLR1 and CLR2 provide more reliable flood inundation estimation than CLR3 and CLR4, which appear to be visually overestimated. With several post-classification adjustments, it is feasible to achieve improved estimations of flood inundation.
Keywords: change detection, flood; synthetic aperture radar

1. Introduction

A frequently used data source in flood analysis is Synthetic Aperture Radar (SAR). In contrast to optical imagery, SAR has the ability to penetrate cloud cover and does not rely on sunlight for illumination. This unique feature makes SAR the most preferred data source for extensive flood mapping, covering large regions and diverse land cover types [1].

The process of flood mapping with SAR imagery can be performed with a single image, taking advantage of either VV or VH polarization. Each has its own characteristics, allowing for customization based on specific needs. For example, VH polarization is generally used for flood extraction in open areas due to its sensitivity to smooth water surfaces. On the other hand, if the area to be mapped is urban, VV polarization is favored due to its heightened sensitivity to vertical structures such as buildings or other infrastructure [2].

Owing to the variations in characteristics, SAR imagery can be considered a primary asset in the application of change detection techniques. Change detection methods are perceived to provide enhanced comprehension relative to maps produced from a single image [3]. Its ability to address outliers caused by temporary water bodies, which lead to significant changes in SAR backscattering, makes it more advantageous for implementation [4].

The log ratio is a widely utilized method for change detection in SAR-based imagery due to its compatibility with amplitude or intensity-based change detection [5]. Fundamentally, the variation of intensity within multi-temporal SAR images can be classified into two principal categories: an increase and a decrease in intensity, and thus, this strategy is considered to deliver the optimal results as it successfully captures both dimensions [6]. Some researchers prefer the use of VV polarization due to its reduced noise considerations compared to cross-polarization, and in particular, this preference is more effective in regions characterized by particular topographical conditions [7][8][9]. Nevertheless, some people choose VH polarization because it is regarded as more appropriate and excellent in distinguishing water bodies from non-water bodies [10]. Considering these strengths, a more effective outcome could potentially be attained by integrating both approaches. The combination of bands with varying characteristics will lead to outputs that offer different insights. This research aims to identify the characteristics of the results from both VH and VV polarization combinations in change detection methods, as well as to evaluate the most reliable combination for detecting flood inundation.

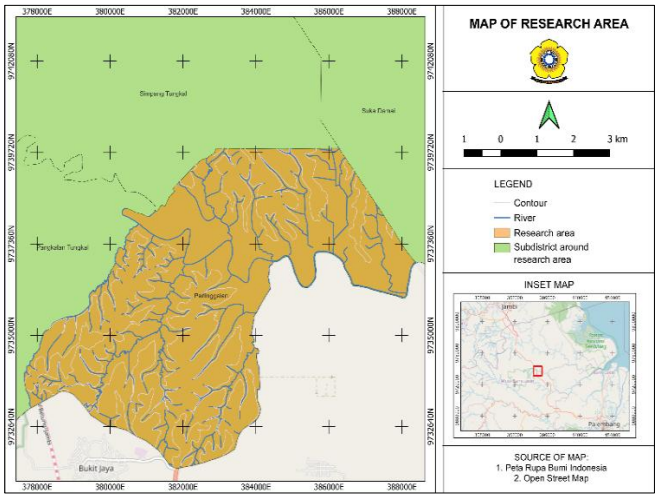

Figure 1. Map of research location

2. Materials and Methods

2.1. Data

The primary data utilized in this research consists of SAR images from Sentinel-1 Ground Range Detected (GRD) mode Interferometric Wide (IW) spatial resolution 10 m x 10 m with dual polarization (VV and VH). The pre-flood data was recorded on February 9, 2025, while the flood data was obtained on April 10, 2025. This research is located in the Peninggalan village, within the Tungkal Jaya District of Musi Banyuasin Regency (Figure 1). The administrative boundary vector of the Peninggalan village at a scale of 1:50000 is applied to define the research location, while the historical field data is used to assess the changes identified by the change detection algorithm.

2.2. Methods

In summary, the procedures involved in this research consist of data preprocessing, collocation, change detection, and data analysis (Figure 2). Preprocessing is performed to reduce distortions and noise in the SAR images, ensuring that the Sentinel-1 GRD data is sufficiently consistent for further analysis and processing. It was applied to images before and during the flood event, considering both cross-polarization (VH) and co-polarization, which is later documented as VH_1, VV_1, VH_2, and VV_2. This preprocessing phase is informed by Selmi [5], Filliponi [11], and Braun [12] as detailed below:

a. Apply Orbit File, updating orbital metadata to enhance the accuracy of both the position and velocity of the satellite.
b. Thermal Noise Removal, aimed at reducing the effects of low-intensity noise and invalid data at the scene edges as well as between sub-swaths by normalizing the backscatter values.
c. Calibration. This procedure involves the transformation of digital pixel values into radiometrically calibrated SAR reflectance values.
d. Speckle Filtering. This procedure is conducted to enhance image quality by reducing speckles. Speckle refers to the visual representation of granular noise found in SAR images.
e. Terrain Correction, aimed at rectifying the geometric distortions that occur using SRTM DEM, ensuring that the image closely represents the geometric reality of the real world.

To enable the effective integration of multi-band usage within Sentinel-1 imagery, collocation is performed. The subsequent process of change detection is carried out by utilizing the log ratio algorithm. This method should be implemented for all possible pairings of SAR images from before and during the flood event.

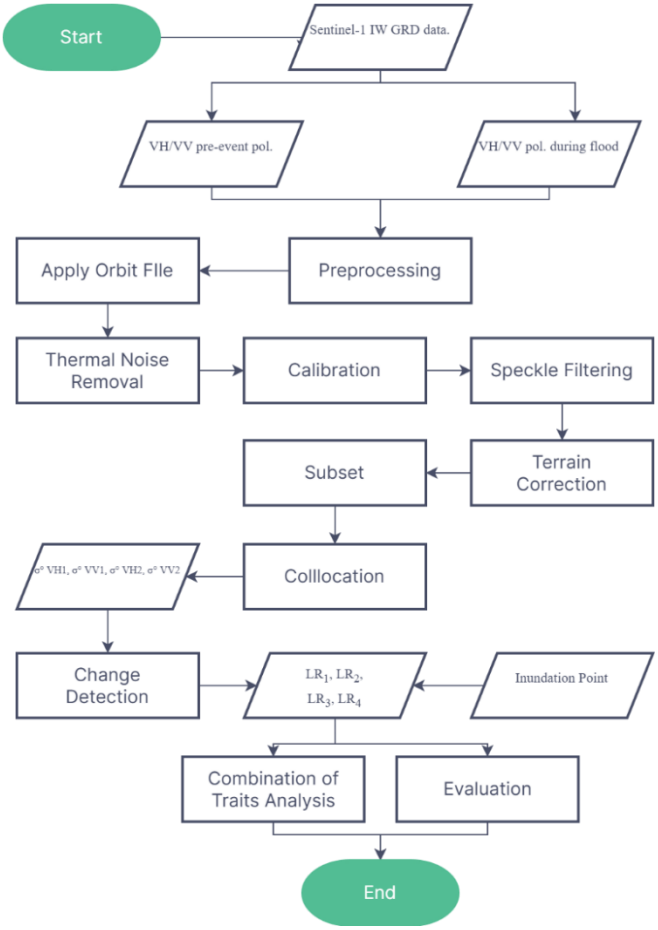

Figure 2. Research flowchart

The change detection output discussed earlier is analyzed in quantitative descriptive analysis to provide a comprehensive overview of the data characteristics. Following the detection of log ratio changes, the outcomes are categorized into water body and non-water body classes through the application of the Expectation Maximization (EM) Cluster Analysis. All these steps, which include preprocessing, collocation, change detection, and image classification, were performed utilizing the Sentinel Application Platform (SNAP), an open-source tool developed by the Copernicus European Space Agency (ESA) for

processing and analyzing earth observation data. The results are then evaluated against the inundation sampling points derived from historical field surveys to determine which combination is the most reliable for flood inundation analysis. This action is carried out using the open-source software Quantum GIS (QGIS).

3. Results and Discussion

3.1. Backscatter Interpretation and Flood Identification

Object identification in SAR imagery is conducted by observing their characteristics and backscatter intensity. High backscatter intensity is usually associated with vertical objects such as trees and buildings, whereas low backscatter coefficients are linked to smooth surfaces or tranquil water. The calibrated images generated in the preprocessing phase, labeled as σ° VV_1, σ° VH_1, σ° VV_2, and σ° VH_2, have a relatively uniform color scheme, as shown in Figure 3. The variations are observable in the flood imagery, where the addition of black hues signifies an increase in the volume of the water body. Statistically, this phenomenon is highlighted by the data presented in Table 1.

Table 1. Statistics of the backscatter coefficient

No.	Statistik	σ^0VH_1	σ^0VV_1	σ^0VH_2	σ^0VV_2
1	Min	0.0008	0.0095	0.0006	0.0072
2	Max	2.8996	26.2838	3.2202	34.2336
3	Range	2.8987	26.2743	3.2196	34.2265

The decrease in minimum intensity, the increase in maximum intensity, and the widening range of values are typical features of flood detection through SAR, which is caused by two scattering mechanisms operating simultaneously in different areas within a single image scene. The specular reflection occurring in open water areas directs the energy away from the sensor, which is further amplified by the high dielectric constant of water, leading to a significantly low backscatter [13][14]. The increase in maximum intensity values is thought to be attributed to the double-bounce backscattering effect, changes in surface roughness , and the interaction of signals with buildings or vegetation that are partially inundated [1][2][4][15]. The extension of the dynamic range is a rational outcome, considering that both mechanisms operate simultaneously within a single scene. Consequently, this leads to greater contrast, more complex classification, and a more challenging thresholding situation [16]. A more distinct visualization of these changes can be observed in Figure 4.

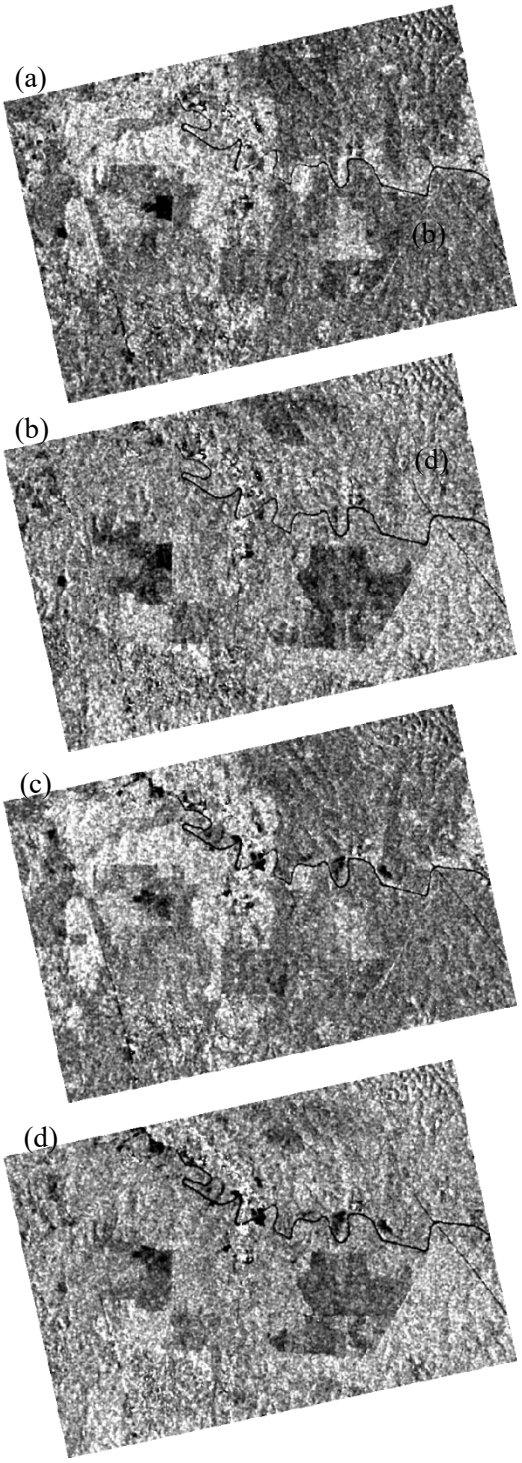

Figure 3. Preprocessed images: (a) VH_1, (b) VV_1, (c) VH_2, and (d) VV_2.

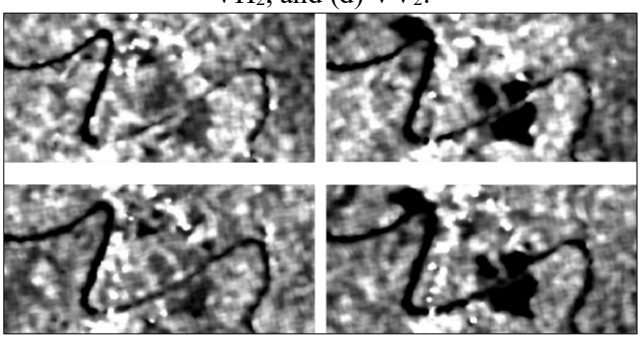

Figure 4. Changes in water bodies during flood event: (a) VH_1, (b) VH_2, (c) VV_1, and (d) VV_2.

3.2. Change Detection

The operator of change detection employed in this study is the log ratio. The log ratio is determined by normalizing the backscatter coefficients from images taken before and during a flood, followed by a logarithmic transformation of the results. As mentioned before, we will use all possible combinations to perform the change detection operator, with the following combination and notation:

$LR_1 = \log (\sigma^\circ VH_1 / \sigma^\circ VH_2)$
$LR_2 = \log (\sigma^\circ VV_1 / \sigma^\circ VV_2)$
$LR_3 = \log (\sigma^\circ VV_1 / \sigma^\circ VH_2)$
$LR_4 = \log (\sigma^\circ VH_1 / \sigma^\circ VV_2)$.

An area that has been detected to have changed will show a ratio value that is either greater than or less than 1. Meanwhile, a log ratio value nearing zero indicates stability. A positive ratio is indicated by a bright hue in the image, while a negative ratio is represented by a dark hue, as illustrated in Figure 5.

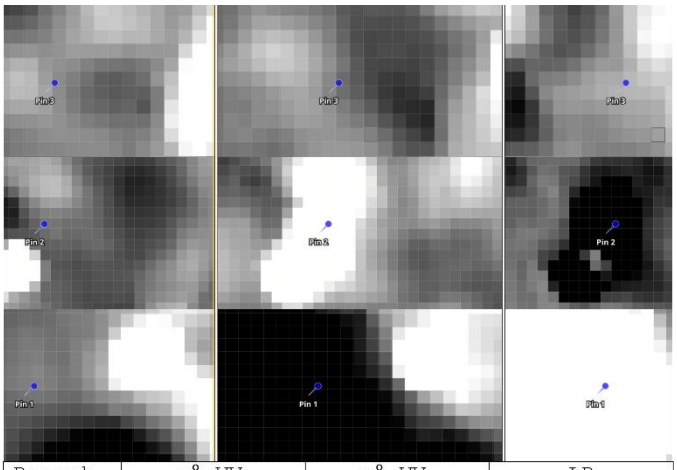

Remark	σ° VV_1	σ° VV_2	LR
Pin 1	0.16181	0.01122	2.66605
Pin 2	0.18429	0.22254	-4.32969
Pin 3	0.19641	0.17984	0.08813

Figure 5. The variation of intensity in SAR images through change detection methods

The differences in the characteristics of VH and VV polarization, along with the variations in image acquisition time, are fundamental to the analysis of change detection. Visually, similar polarization combinations exhibit nearly identical image textures. The key difference lies in the fact that the LR_1 in Figure 6a yields darker image hues when compared to the LR_2 in Figure 6b, and it is the darkest when contrasted with the combination of LR_3 in Figure 6c and the combination of LR_4 in Figure 5d. In contrast to 1st and 2nd combinations, 3rd and 4th combinations illustrate particular land cover patterns within their image textures (Figure 6).

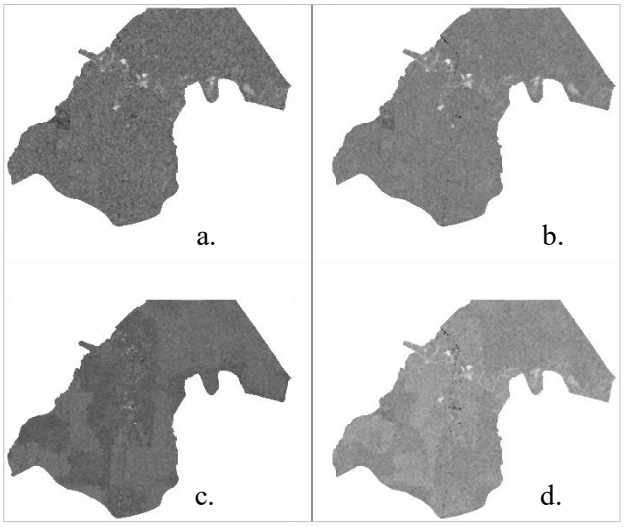

Figure 6. Log ratio images visualization

This log ratio application, by default, has adopted a lower threshold of -2 and an upper threshold of 2, which has been applied across all combinations. Thus, a change is deemed significant within the defined parameters. As shown in Figures 7 and 8, changes are visually marked by bright and dark hues in the LR image.

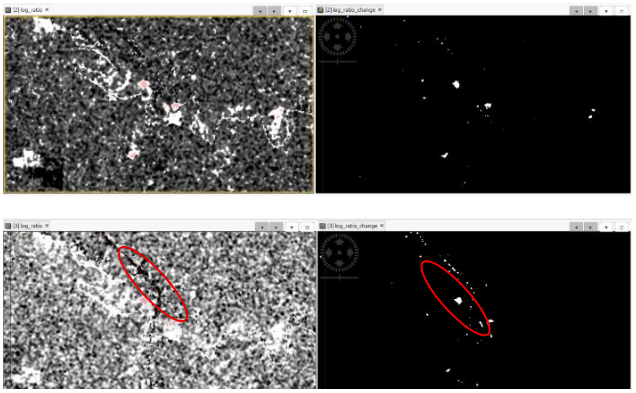

Figure 7. LR and LRC of LR_1 and LR_2

In LRC_1, the algorithm considers only 676 cells that have shown a significant change. Among these, 656 cells have shown positive changes, while 20 cells have shown negative changes. This is corroborated by the positive mean and median values (Table 2), which reflect a positive trend in the changes. In LRC_2, a total of 835 cells were identified as having changed, consisting of 490 cells with positive changes and 245 cells with negative changes. Unlike LRC_1, the darker hues identified as changes are also apparent in the LR image due to the considerable amount of negative change values. Some of these are highlighted with red borders in the image.

Table 2. Statistics of LRC

Statistics	LRC_1	LRC_2	LRC_3	LRC_4
Count	676	835	44,620	57,834
Mean	2.30	0.84	2.23	-2.17
Median	2.35	2.20	2.12	-2.11
Minimum	-2.83	-5.62	2.00	-7.04
Maximum	3.54	4.20	5.96	2.15
Change (+)	656	490	44,620	2
Change (-)	20	245	0.00	57,832

Changes in LRC_3 are characterized by a predominantly bright appearance in the LR image, which does not reflect any negative change values, amounting to 44,620 cells (Figure 6). Due to this inclination, this combination might be useful for identifying positive changes. The final combination, LRC_4, detects the highest number of changes compared to the other combinations, totaling 57,834 cells. In contrast to LRC_3, the detection results of this combination are largely dominated by negative changes, with 57,832 cells showing negative values, while only 2 cells were detected as positive. The negative trend is further corroborated by the negative mean and median values. Like LRC_3, based on this trend, LRC_4 may be suitable for detecting negative changes.

Visually, the bright patterns observed in LR across all image combinations can be interpreted as flood inundation. However, given the threshold applied, it appears challenging to ascertain whether the changes are positive or negative, directly associated with the flood inundation. In comparison to the single image during the flood shown in Figure 3, only LRC_3 demonstrates a comparable pattern, aligns with the river flow pattern, and disperses in the surrounding area, although, on the other hand, it appears to be overestimated. Therefore, selecting the appropriate.

The threshold is essential for enhancing the precision of the generated map [17][15]. Moreover, a technique that satellite imagery-based flood interpretation should consider is hydrological connectivity patterns and types of land cover [2][18]. In contrast to LRC_4, it appears to be a false alarm, as it does not connect with the hydrological pattern; the resulting pattern is more linked to the residential zone (yellow border in Figure 8).

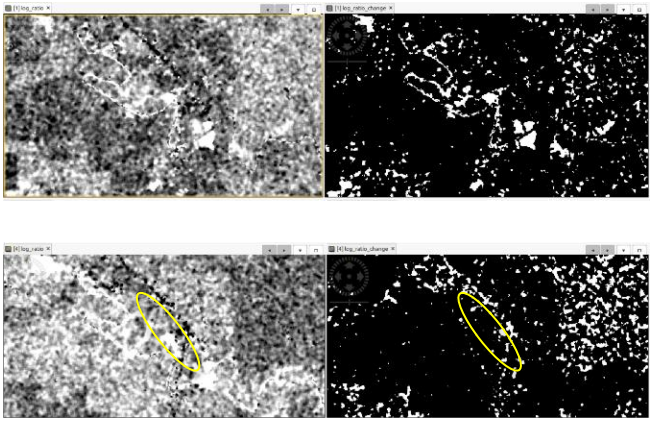

Figure 8. LR and LRC of LR_3 and LR_4

3.3. Evaluation

The dynamics of the Earth's surface during a flood are of great importance to consider, as it will affect the characteristics of the SAR signal backscatter. Inundation in urban areas and vegetation results in the phenomenon of double-bounce scatter, which is caused by the complex interactions between radar signals, structures, or trees, and the water itself [2][15]. Furthermore, inundation impacts the changes in surface roughness, potentially causing extreme specular reflections that will affect backscatter intensity [19]. Flooding, often accompanied by high rainfall intensity, can also affect soil moisture levels, and high moisture levels correspond to a high dielectric constant [20]. This, in turn, influences the variations in backscatter intensity, considering that SAR is sensitive to these dielectric characteristics [21].

This study's evaluation involves comparing the classification results from EM Cluster Analysis with single images recorded during flooding. Furthermore, a comparison is carried out among the classification results based on inundation sample points obtained from historical data in the field. The results are presented in the following Figure 9.

According to the image, it is apparent that LR_4 and LR_3 sequentially generate the most extensive flood inundation classes, with areas of 501.53 ha and 686.98 ha, respectively (Table 3). A visual assessment reveals a substantial potential for overestimation, as indicated by the numerous bright areas interpreted as water bodies. This phenomenon is suspected to arise from the double-bounce effect, resulting from either temporary flooding of vegetated areas or changes in surface roughness, which distort the backscatter signal [8].

Table 3. The extent of the classified log ratio (CLR)

Class output	Area (Ha)	Count (polygon)
CLR_1	352.81	1,842
CLR_2	229.93	1,341
CLR_3	501.53	1,524
CLR_4	686.98	2,083

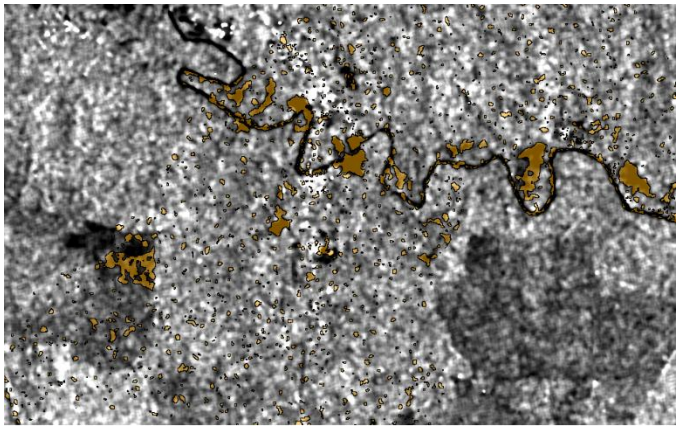

(a)

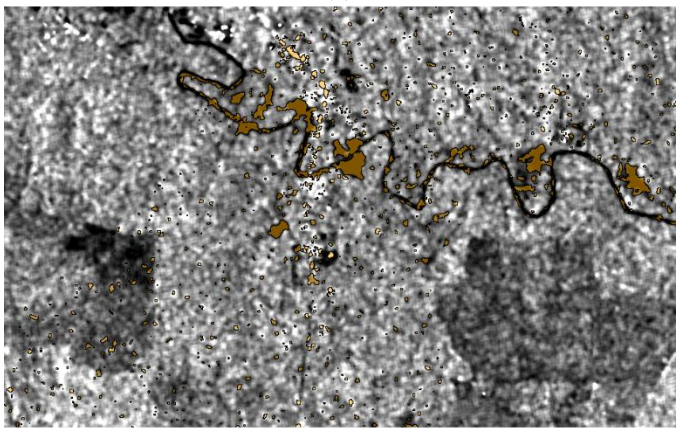

(b)

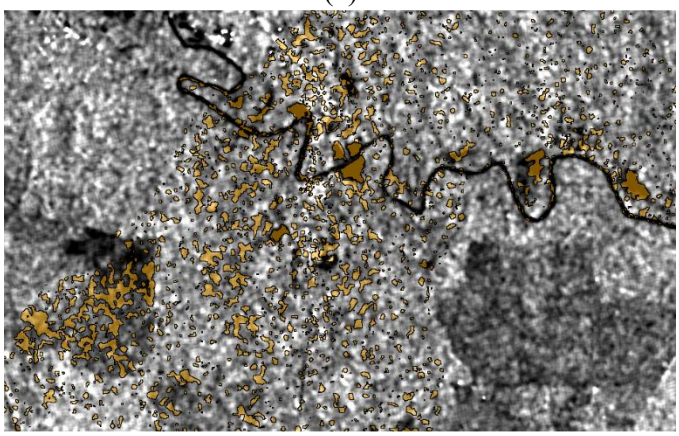

(c)

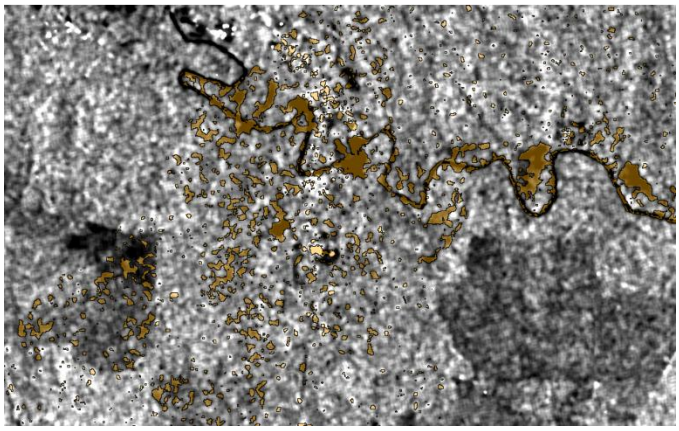

(d)

Figure 9. Evaluation of flood inundation according to LR_1 (a), LR_2 (b), LR_3 (c), and LR_4 (d)

CLR_1 (Fig. 9a) and CLR_2 (Fig. 9b) exhibit narrower extents of 352.81 ha and 229.93 ha, respectively. When compared to CLR_3 (Fig. 9c) and CLR_4 (Fig. 9d), these classifications show a reduced presence of noise. The distortions that occur are predominantly in residential areas along the main roads, indicating that this combination is seemingly more responsive to this specific land cover type. The LR_1 combination seems to delineate water bodies with a slightly greater extent than LR_2. This is likely attributed to the cross-polarization characteristics, which tend to include more noise than co-polarized data [7].

This investigation has also involved the consolidation of the four classification results, resulting in a new geometric feature that represents the overlapping area and inherits attributes from all intersecting input layers [22]. The output (latter called CLRI) can be observed in Figure 10. The area derived from this procedure is the least extensive, while simultaneously demonstrating the minimal occurrence of errors in detecting non-water objects.

The classification results were also evaluated with data from historical field surveys. A total of 111 flood inundation points have been recorded for subsequent overlay analysis. The results are displayed in Table 4.

Tabel 4. evaluation of classification results

Result	CLR1	CLR2	CLR3	CLR4	CLRI
Confirmed	73	75	102	58	30
Persentage	65.77	67.57	91.89	52.25	27.03

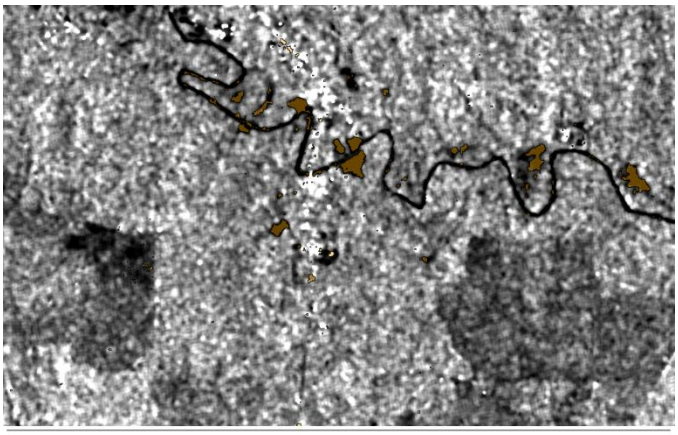

Class output	Area (Ha)	Count (polygon)
CLRI	59.08	250

Figure 10. Intersection layer

CLR_3 has verified the presence of flooding at 102 sites, achieving a detection rate of 91.89% for the test points. The number of estimated inundations that are unassociated and distant from the river raises concerns that the results may represent false alarm change pixels. This situation is a consequence of the intricate interactions between SAR signals and certain types of land cover, including vegetated areas.

A similar pattern is observed in CLR_4. The results of the classification are only aligned with 58 test points,

and this does not correspond proportionately to the amount of inundation that has occurred. By integrating cross and co-polarization through the log ratio operator, it seems to accentuate the VH band, which is indicative of water reflection. However, this could result in an overestimation [23][24]. Moreover, it generates more flooded pixels than the combinations of the same polarizations.

CLR_1 and CLR_2 demonstrate a commendable ability to detect inundation, achieving rates of 65.77% and 67.57%, respectively. The use of the same polarization combination appears to effectively reduce speckle noise in SAR images. This may elucidate why some researchers prefer the combination of LR_1 and LR_2 over the two previous combinations. Nevertheless, undeniable inaccuracies are still apparent, such as the erroneous labeling of dwelling attributes as flood inundation. To enhance reliability, it is essential to undertake several additional measures, including the removal of pixels identified as residential, eliminating permanent water bodies, discarding areas with slopes exceeding 5%, and excluding areas smaller than 8 pixels [9].

4. Conclusion

Essentially, the log ratio output across all combinations is capable of displaying a sufficiently contrasting estimation of flood inundation in comparison to the surrounding areas. However, LR_3 and LR_4 still exhibit patterns that correspond to specific land cover types. Changes in LR_1 and LR_2 can effectively capture both decreases and increases in intensity, while LR_3 only captures increases in intensity, and the intensity changes in LR_4 are predominantly characterized by decreases in intensity. CLR_1 and CLR_2 provide more reliable flood inundation estimation than CLR_3 and CLR_4, which appear to be visually overestimated. With several post-classification adjustments, it is feasible to achieve improved estimations of flood inundation.

Acknowledgement

The study could not have been conducted without the datasets provided by the European Space Agency, specifically the Sentinel-1 Synthetic Aperture Radar.

References

[1] J. Zhao, Z. Xiong, and X. X. Zhu, "UrbanSARFloods: Sentinel-1 SLC-based benchmark dataset for urban and open-area flood mapping," in *2024 IEEE/CVF Conference on Computer Vision and Pattern Recognition Workshops (CVPRW)*, IEEE, Jun. 2024, pp. 419–429. doi: 10.1109/CVPRW63382.2024.00047.

[2] Z. Wang, C. Zhang, and P. M. Atkinson, "Combining SAR images with land cover products for rapid urban flood mapping," *Front. Environ. Sci.*, no. October, pp. 1–12, 2022, doi: 10.3389/fenvs.2022.973192.

[3] M. Siddique and T. Ahmed, "CCD-Conv1D: A deep learning based coherent change detection technique to monitor and forecast floods using Sentinel-1 images," *Remote Sens. Appl. Soc. Environ.*, vol. 37, pp. 1–17, 2025, doi: 10.1016/j.rsase.2024.101440.

[4] D. Amitrano, G. Di Martino, A. Di Simone, and P. Imperatore, "Flood detection with SAR : A review of techniques and datasets," *Remote Sens.*, vol. 16, no. 656, pp. 1–38, 2024, doi: https://doi.org/10.3390/rs16040656.

[5] L. Selmi, "Flood mapping using the Sentinel-1 imagery and the ESA SNAP S1 Toolbox," 2021.

[6] H. Zhuang, Z. Tan, K. Deng, and H. Fan, "It is a misunderstanding that log ratio outperforms ratio in change detection of SAR images," *Eur. J. Remote Sens.*, vol. 52, no. 1, pp. 484–492, 2019, doi: 10.1080/22797254.2019.1653226.

[7] M. S. Ruuhulhaq, "Multi-temporal Sentinel-1 SAR image utilization for urban flood-affected public facility identification : a case study in Bandung City," *Geomatika*, vol. 30, no. 02, pp. 111–120, 2024.

[8] A. M. Alawiyah and H. Harintaka, "Identification of flood inundation in DKI Jakarta area using Sentinel-1 Satellite Imagery," *JGISE J. Geospatial Inf. Sci. Eng.*, vol. 4, no. 2, pp. 95-101, 2021, doi: 10.22146/jgise.68353.

[9] R. Dhanisa, J. Sampurno, and R. Perdhana, "The Sentinel-1 SAR application for flood detection in Sandai, Ketapang, West Kalimantan," *J. Ilmu Lingkung.*, vol. 22, no. 3, pp. 672–677, 2024, doi: 10.14710/jil.22.3.672-677.

[10] F. A. Budiarto and F. Bioresita, "Utilization of Sentinel-1 SAR imagery and change detection approach method for spatial distribution analysis of flood areas and affected areas (case study: floods of North Aceh District 2022)," *JGISE J. Geospatial Inf. Sci. Eng.*, vol. 6, no. 2, pp. 153–162, 2023, doi: 10.22146/jgise.87585.

[11] F. Filipponi, "Sentinel-1 GRD preprocessing workflow," in *3rd International Electronic Conference on Remote Sensing*, MDPI,

2019, p. 1-4. doi: 10.3390/ecrs-3-06201.
[12] A. Braun, *Sentinel-1 toolbox time-series analysis with Sentinel-1*. SKYWATCH ESA, 2021.
[13] F. Bioresita, N. Hayati, M. G. R. Ngurawan, and M. Berliana, "Integrating InSAR coherence and backscattering for identification of temporary surface water, case study : South Kalimantan flooding, Indonesia," in *2022 24th ISPRS Congress on Imaging Today, Foreseeing Tomorrow, Commission III , 6-12 June 2022*, Nice, France, 2022, pp. 6–11. doi: https://doi.org/10.5194/isprs-archives-XLIII-B3-2022-33-2022.
[14] S. Grimaldi, J. Xu, Y. Li, V. R. N. Pauwels, and J. P. Walker, "Flood mapping under vegetation using single SAR acquisitions," *Remote Sens. Environ.*, vol. 237, pp. 1–20, 2020, doi: 10.1016/j.rse.2019.111582.
[15] G. Schumann, L. Giustarini, A. Tarpanelli, B. Jarihani, and S. Martinis, "Flood modeling and prediction using earth observation data," *Surv. Geophys.*, vol. 44, no. 5, pp. 1553–1578, 2023, doi: 10.1007/s10712-022-09751-y.
[16] S. Schlaffer, M. Chini, L. Giustarini, and P. Matgen, "Probabilistic mapping of flood-induced backscatter changes in SAR time series," *Int. J. Appl. Earth Obs. Geoinf.*, vol. 56, pp. 77–87, 2017, doi: 10.1016/j.jag.2016.12.003.
[17] T. A. Gasica, F. Bioresita, and A. Murtiyoso, "Identification of temporary surface water using Sentinel-1 SAR data, case study: Sentani flash flooding, Indonesia," *Int. Arch. Photogramm. Remote Sens. Spat. Inf. Sci.*, vol. XLIII-B3-2, pp. 55–59, 2020, doi: https://doi.org/10.5194/isprs-archives-XLIII-B3-2020-55-2020.
[18] I. Prasasti, I. Carolita, A. E. Ramdani, and I. Risdiyanto, "The study of ALOS PALSAR data application for soil moisture estimation," vol. 9, no. 2, pp. 102–113, 2012.
[19] N. Bhogapurapu, S. Dey, S. Homayouni, A. Bhattacharya, and Y. S. Rao, "Field-scale soil moisture estimation using sentinel-1 GRD SAR data," *Adv. Sp. Res.*, vol. 70, pp. 3845–3858, 2022, doi: https://doi.org/10.1016/j.asr.2022.03.019.
[20] Z. Xiaomin, Z. Hongchao, and F. Jinyun, "A robust and efficient method for vector map overlay," *J. Remote Sens.*, vol. 16, no. 3, pp. 448–466, 2012.
[21] M. A. Clement, C. G. Kilsby, and P. Moore, "Multi-temporal synthetic aperture radar flood mapping using change detection," *J. Flood Risk Manag.*, vol. 11, pp. 152–168, 2017, doi: 10.1111/jfr3.12303.
[22] H. Ashilah and U. Lasminto, "Enhancing food detection in Surabaya: A comparative study of VV and VH polarizations with Sentinel-1 Data," *J. Civ. Eng.*, vol. 40, no. 1, p. 89, 2025, doi: 10.12962/j20861206.v40i1.22329.